Synthesis of Nano-structured Ni-Co-Al Hydrotalcites and Derived Mixed Oxides

M Abdus Salam[a], Ye Lwin[b], Suriati Sufian[c]

Chemical Engineering Department, Universiti Teknologi PETRONAS,
Bandar Sri Iskandar, 31750 Tronoh, Perak, Malaysia.

[a]salam.bcsir@gmail.com , [b]dryelwin@petronas.com.my, [c]suriati@petronas.com.my

Abstract. Nano-structured hydrotalcite-like compounds that contain nickel, cobalt and aluminum have been synthesized by conventional coprecipitation method without using any surfactants or templating agents. The structure and morphology of the coprecipitated nano hydrotalcites and its derived mixed oxides were characterized by powder X-ray diffraction (XRD), Fourier-transformed Infrared (FTIR) spectroscopy, field-emission scanning electron microscopy (FESEM), high resolution transmission electron microscopy (HRTEM), and nitrogen adsorption-desorption techniques. The results show that the synthesized materials exhibited micro-meso-pore networks. The cobalt-rich calcined hydrotalcites are generally amorphous, having a coral-like morphology whereas nickel-rich hydrotalcites show hexagonal plate-like morphology. The presence of nickel in mixed oxides catalyzed the reduction of Co-Al-O spinels. The Fast Fourier Transform (FFT) analysis of HRTEM revealed the inter planner distances of the crystal of hydrotalcite.

Introduction

Synthesis methods play an important role to produce nano-sized crystals of hydrotalcite. In addition, kinetic factors also control the growth of the crystal. In synthesizing nanostructured hydrotalcite, some researchers suggest that through coprecipitation, separation of the nucleation and crystal growth could be done to give uniform crystallite size [1, 2, 3]. Subsequently, they used coprecipitation with high supersaturation condition, such as in colloid mill, and separate aging to synthesize the hydrotalcites. The size and shape of the nano-particles can also be controlled by pH, temperature, types of salt and their ionic strength, as well as ratio of the metal cations [4-6]. Moreover, the increase in mixing rate tends to decrease the particle size [7]. Structural modifying agents or templating agents also influence the formation of nano-structured hydrotalcites [8].

The standard formula of hydrotalcite-like compounds or structures (HTlcs) can be written as $[M^{II}_{1-x}M^{III}_{x}(OH)_2][A^{q-}_{x/q}\cdot nH_2O]$, where $[M^{II}_{1-x}M^{III}_{x}(OH)_2]$ and $[A^{q-}_{x/q}\cdot nH_2O]$ represent the layer and the interlayer composition, respectively [3, 9, 10]. M^{II} and M^{III} are divalent and trivalent metal cations respectively, A^{q-} is a q-valent anion, and x varies between approximately 0.25 and 0.33 [11, 12]. Multi-elemental HTlcs (binary or ternary) are identified as promising precursors of mixed oxides with a homogenous distribution of metals [13]. Partial substitution of the metals can be used to refine the properties of the material. At higher temperatures, HTlcs are transformed to mixed metal oxides, which serve as good catalysts and adsorbents because of their large surface area, high metal dispersions, and good thermal stability [14, 15 ,16]. In this work, the conventional homogeneous coprecipitation under the low supersaturation and variable pH conditions are investigated during the synthesis of the nanosized hydrotalcite particles.

Methodology

Samples of Ni-Co-Al HTlcs with different molar ratios were prepared by coprecipitation method from metal nitrate precursors where Na_2CO_3 was used as the precipitating agent. The method was similar to the one described for the preparation of Cu-Al HTlcs [17]. The Ni:Co:Al molar ratios used in the solutions were 3:0:1, 2:1:1, 1:2:1, and 0:3:1, respectively. Each solution was dropped into a 0.5 M sodium carbonate solution maintained at 45°C. The pH was varied initially from 12.5 to 9 after the

completion of the addition of nitrates solution. Later, the precipitate was filtered and washed several times with warm distilled water to remove excess Na^+ and NO_3^- ions. The filtered precipitates were dried in an oven overnight at 110°C. The developed materials were calcined in a furnace at 500°C for two hours to obtain mixed oxides. The dried precipitates (uncalcined) and the calcined samples are designated by NCAH-xyz and NCAH-xyzc, respectively, where NCAH stands for Ni-Co-Al HTlcs, xyz stands for the molar ratios x:y:z of Ni:Co:Al, and c represents the calcined samples.

The crystal structure of the uncalcined and calcined HTlcs were analysed by powder X-ray diffraction (XRD) technique using a Bruker D8 advanced diffractometer with Cu-K$_\alpha$ radiation (λ = 0.154 nm). The FTIR spectra of uncalcined and calcined HTlcs were obtained by using a Nicolet 380 FTIR spectrometer (SHIMADZU) in the range of 4000–400 cm^{-1} using KBr. For microscopy analysis, the surface morphology was studied by using n field-emission scanning electron microscope (FESEM), CARL Zeiss Supra 55VP instrument at an operating voltage of 0.1–30 kV. High resolution transmission electron microscopy (HRTEM) was performed by using a CARL Zeiss LIBRA^R 200FE electron microscope with an acceleration voltage of 200 kV. The specific BET surface areas (S$_{BET}$) were determined by running nitrogen adsorption-desorption using a Micromeritics ASAP 2020 sorptometer. The pore volumes were calculated by using the *t*-plot method of De Boer. The reducibility of the calcined samples was studied by temperature-programmed reduction (TPR) using a Thermo Finnigan TPD/R/O 1100 instrument. A 20–25 mg sample was reduced by a 5% H$_2$-in-N$_2$ flowing at 20 ml/min, with heating rate of 10 K/min up to 1000°C.

Results and Discussion

The X-ray diffraction (XRD) patterns of uncalcined hydrotalcites are shown in Fig. 1(a). The group of peaks at 2θ = 11.52°, 22.84°, and 35° corresponding to diffractions by (003), (006), and (009) crystal planes, respectively. This indicates the typical hydrotalcite-like layered structure (JCPDS 15- 0087). The peaks at 38°, 46°, and 61° represent (105), (108), and (110) plane, respectively, of the hydrotalcite structure. The average crystallite sizes of the samples were determined by the Scherrer equation. The results are given in Table 1 where the unit cell parameters and (009) crystal planes indicate the typical hydrotalcite-like layered structure.
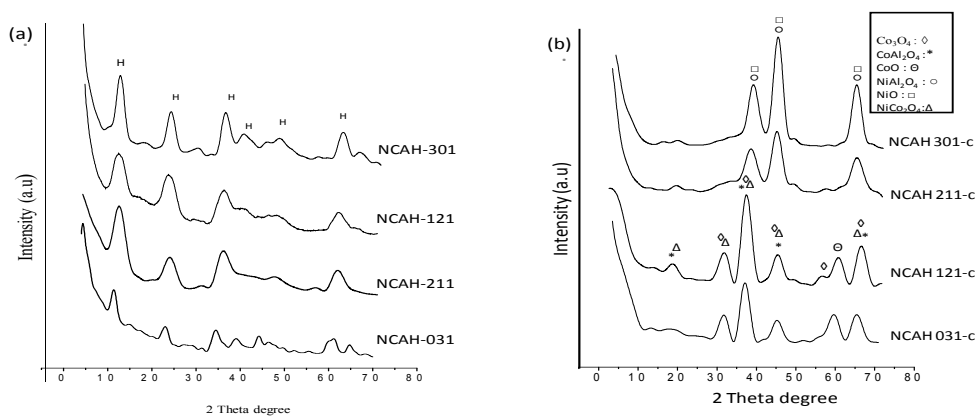
Fig.1: XRD pattern of (a) uncalcined and (b) calcined Ni-Co-Al hydrotalcite at different molar ratios.

The relative dimensions of the cell parameters correspond to the rhombohedral 3R stacking sequence of the hydrotalcite crystals [17]. The *a*-parameter, which represents the average cation-cation distance within the brucite-like layers, increases with increase cobalt content due to the larger ionic radius of Co^{2+} (0.74 Å) than Ni^{2+} (0.72 Å). The *c*-parameter indicates the relation to the thickness of the brucite-layer and the

Table 1: X-ray diffraction data of Ni-Co-Al hydrotalcites

Sample	Cell parameter		Crystal size (nm)	*d*-spacing (nm)
	a (nm)	*c* (nm)		
NCAH-301	0.300	2.32	4.39	0.782
NCAH-211	0.301	2.32	3.95	0.779
NCAH-121	0.303	2.31	4.16	0.767
NCAH-031	0.311	2.29	2.79	0.773

interlayer distance. Through investigation, Ni-rich HTlcs show larger crystallite size than Co rich samples. This is in good agreement with previous investigations [19, 20]. The *d*-spacing (003) of Ni-rich HTlcs is generally higher than Co-rich samples.

The XRD patterns of the calcined HTlcs, as shown in Fig. 1(b), indicate that the precursor HTlcs were decomposed, leading to the various oxide derivatives. For samples containing both Co and Ni, the oxides are mainly of the spinel phases, with the characteristic diffraction peaks of $NiCo_2O_4$ (JCPDS 20–781), in addition to individual spinels: $CoAl_2O_4$ (JCPDS 82–2246), $NiAl_2O_4$ (JCPDS 10-0339), and Co_3O_4 (JCPDS 42-1467). It can be generally seen that the Ni-rich samples have higher crystallinity than the Co-rich samples.

The SEM and FESEM images of some calcined and uncalcined samples are shown in Fig. 2. The image of uncalcined NCAH-211, as shown in Fig. 2(a) is a representative of all uncalcined samples. The uncalcined samples show hexagonal plate-like and coral-like morphology can be seen in Fig. 2(b) and (c), respectively. : FESEM image of NCAH-031are generated in sharp and in more uniform through calcination due to removal of impurity and water and strongly bonded hydroxyl. Porous materials with plate-like particles have geometry of openings between plates. Higher content of cobalt, which has larger ionic radius than nickel, distorts the hydrotalcite structure resulting in the coral-like morphology.
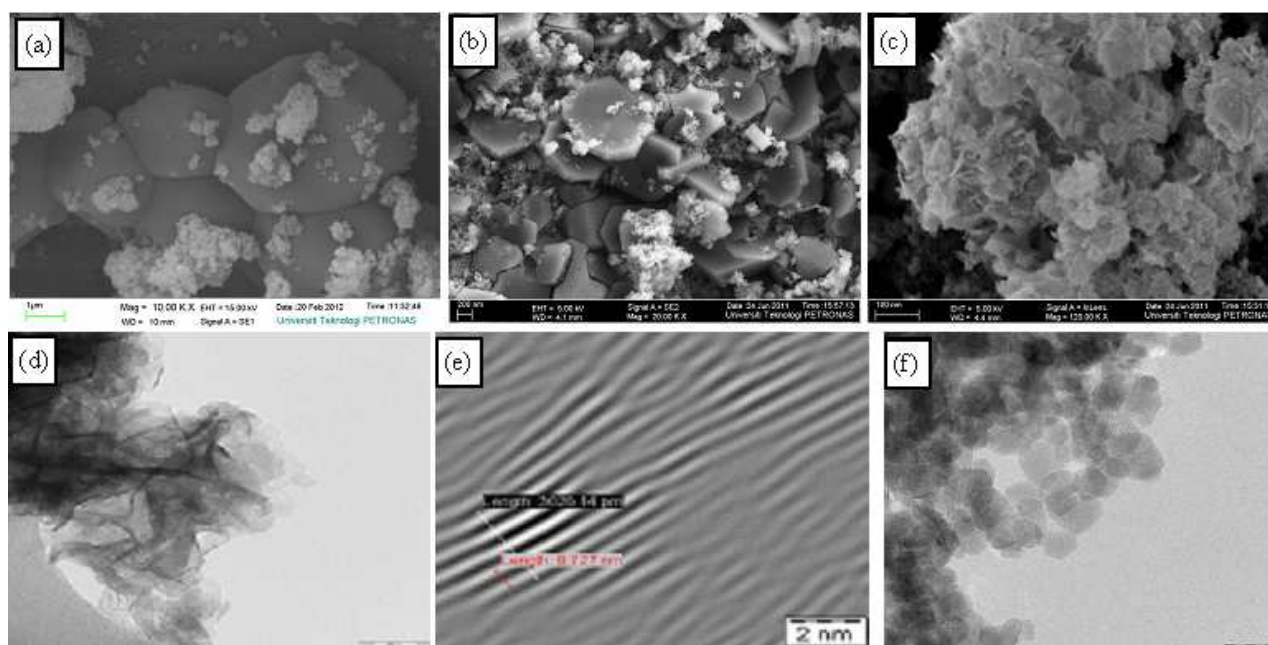
Fig.2: (a) SEM image of coral-like and hexagonal morphology of uncalcined NCAH-211; (b) FESEM images of plate-like hexagonal sheets of calcined NCAH-211c, (c) coral-like morphology of calcined NCAH-031c (d) TEM image of uncalcined NCAH-211 (e) FFT of image 'd' showing inter-planer distances of (003) plane. (f) TEM image of hexagonal particle of NCAH-121c.

TEM micrograph of uncalcined NCAH-211 is shown in Fig.2(d) while typical HRTEM images in Fig. 2(e). Fig.2(d) reveal the presence of planes with an inter-planar distance of about 0.7 nm, that of the (003) planes, confirming the formation of hydrotalcites. Fig. 2(f) shows the nano-scale hexagonal plate-like particles. The sizes of the particles are in the range 13-21 nm.

The FTIR spectra of uncalcined hydrotalcite samples are shown in Fig. 3(a). The hydrotalcite structure can be identified by three vibrational infrared bands corresponding to hydroxyl groups, interlayer water and interlayer anions respectively. The broad band at high frequency range (4000-3000 cm^{-1}) is due to the stretching of hydroxyl groups from the layers and interlayer water molecules.This vibration mode seems to shift to higher wave numbers with an increase in cobalt content, with increased broadening . A narrower absorption band at about 1635 cm^{-1} is due to the bending mode of the interlayer water molecule [21]. A sharp band at 1385 cm^{-1} can be assigned to the stretching vibration of the interlayer carbonate [22]. The week band at around 2345 cm^{-1} are due to the equipment detection of atmospheric CO_2.

The nitrogen adsorption-desorption isotherms of Ni-Co-Al HTlcs with different molar ratios showed type IV isotherm which indicates mesoporous nature of the samples. Fig. 3(b) shows a typical isotherm curve of uncalcined NCAH-301. The isotherm begins with micropores and then capillary condensation occurred in the mesopores at high relative pressures. As a result, the isotherm went upward with increased quantity adsorbed. The desorption started almost immediately after completion of adsorption with the characteristic hysteresis loop H_3, which is an indication of non-rigid aggregation of plate-like particles forming slit-like pores.
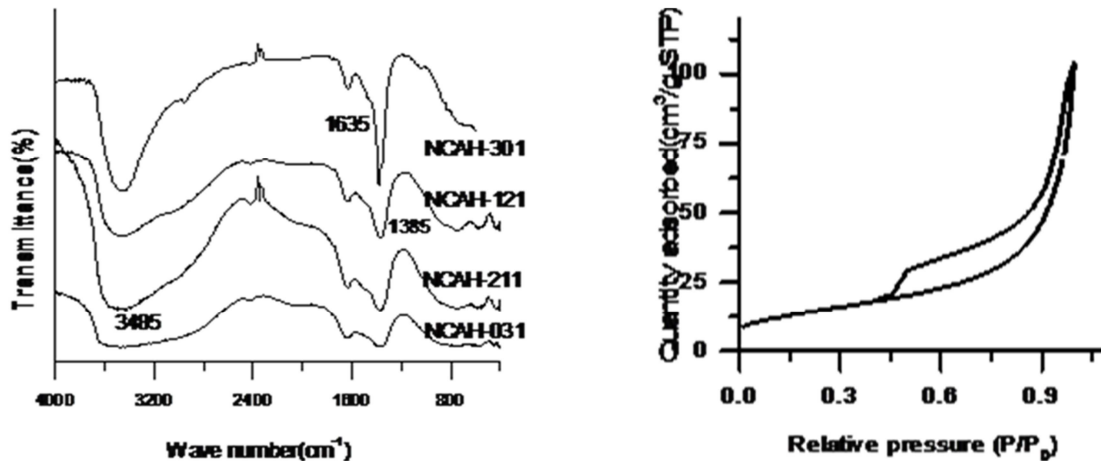
Fig.3: (a)FTIR spectra and (b) isotherm curve of the uncalcined materials.

The loop closes at around 0.4 to 0.5 relative pressure (P/P_o) ranges with a small plateau, which attributes to the micropore -mesopore network structure of these samples. The textural properties obtained from the BET analysis are summarized in Table-2. Generally, the BET surface areas (S_{BET}) of the Ni-Co-Al Hydrotalcites were observed to decrease after calcinations due to the partial collapse of HTlcs structure and agglomeration of particles. Only Ni-Co-Al 121HTlcs shows increased surface area after calcination due to the formation of microspores and mesopores caused by removal of CO_2 and water during calcination.

Table 2: Textural properties of Ni-Co-Al

Sample	Surface area ($m^2 g^{-1}$)	Pore size (nm)	Pore volume ($cm^3 g^{-1}$)
NCAH-301	76.50	8.49	0.162
NCAH-301c	55.15	13.36	0.184
NCAH-211	147.53	8.97	0.331
NCAH-211c	74.56	14.72	0.275
NCAH-121	87.86	6.05	0.132
NCAH-121c	111.03	12.85	0.356
NCAH-031	113.09	7.94	0.224
NCAH-031c	82.68	15.39	0.318

The results of TPR on the calcined Ni-Co-Al HTlcs are shown in Fig. 4. Two reduction peaks for NCAH-031c are observed at 312°C and 673°C with respective broad shoulders at 390°C and 729°C. The first reduction peak with its broad shoulder represents successive reduction of Co^{3+} and Co^{2+} from Co_3O_4 spinel: $Co_3O_4 \rightarrow CoO \rightarrow Co^0$ [24, 25]. The H_2 consumption for these two successive steps is about 32% of the total hydrogen consumption. The second peak and its shoulder represent the parallel and series reduction of Co^{3+} and Co^{2+} from Co-Al-O spinels: $Co_2AlO_4 \rightarrow CoAlO_3$ and $CoAl_2O_4 \rightarrow Co^0$. The H_2 consumption of this combined step is about 68% of total H_2 consumption.

The TPR profile of NCAH-301c indicates a peak at 360°C and a shoulder around 520°C. The peak at 360°C is due to reduction of Ni from free NiO phase, for which about 50% of H_2 was needed. The weak and broad shoulder at 520°C is due to reduction of the $NiAl_2O_4$ spinel [26], where NiO associated with alumina is reduced.
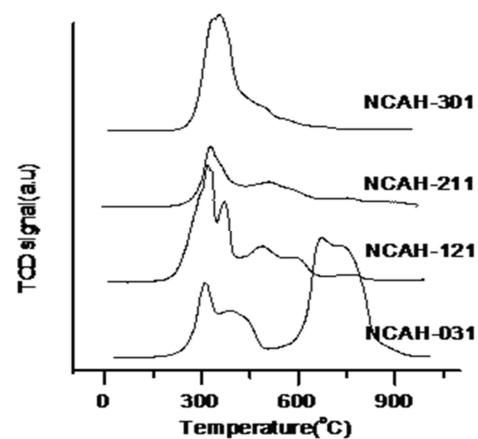
Fig. 4: TPR profiles of mixed oxide

The ternary calcined hydrotalcites, NCAH-121c and NCAH-211c, showed different reduction patterns from those of binary hydrotalcites. Both samples first reduced at about 350°C due to the reduction of Co (III & II) oxides that are influenced by Ni to reduce at slightly higher temperature, near which NiO is reduced. The TPR patterns for Ni-rich and Co-rich ternary HTlcs showed a weak peak at temperature range 507-550°C due to the reduction of Ni and Co from $NiCo_2O_4$ phase with peak overlapping. The weak and broad peaks at reduction temperature range of 600°C to 750°C correspond to the reduction of Ni and Co (II) from spinel-like phases of $CoAl_2O_4$ and $NiAl_2O_4$. The closeness of the reduction peaks in the ternary hydrotalcites indicates that strong interaction exists between Ni and Co species and that Ni acts as a catalyst for reduction of Co-Al-O spinels.

Conclusion

Nano-structured Ni-Co-Al HTlcs were synthesised by homogeneous coprecipitation at variable pH. The calcination of the hydrotalcites generated highly interactive mixed oxides with hydrotalcite skeletal structure. The calcined samples showed hexagonal plate-like morphology for Ni-rich samples and coral-like morphology for Co-rich samples. The particle sizes of the calcined Ni-Co-Al HTlcs range from about 10 to 20 nm.

Acknowledgements

References:
[1] K.Setshedi, J. Ren, O.Aoyi and M.S. Onyango, Int. J. Phy. Sciences 7(1) (2012) 63 – 72
[2] Y.Zhao, F. Li, R. Zhang, D. G. Evans, and X. Duan, Chem. Mater. 14(2002), 4286.
[3] D.G. Evans, R.C.T. Slade, in: X. Duan, D.G Evans (Eds.), Layered Double Hydroxides. Springer, New York, 2006, p. 1–87.
[4] Y.Arai, M. Ogawa, Appl. Clay Sci. 42(2009),601.
[5] H. Itoh, T. Sugimoto, J. Colloid interface Sci. 265(2003), 283.
[6] M.Tominga, M. Matsumoto, K. Soejimaand, I. Taniguchi, J. Colloid Interface. 299(2006), 761.
[7] R. Xu and H. C. Zeng, Chem. Mater. 13(2001), 297.
[8] H. Wang, G. Fan, C. Zheng, X. Xiang, F. Li, Ind. Eng. Chem. Res. 49(2010), 2759.
[9] V. Rives, Mater. Chem. Phys. 75(2002), 19.
[10] C. Gabriele, P. Siglinda, Microporous Mesoporous Mater. 107(2008), 3.
[11] P.S. Braterman, Z.P. Xu, F. Yarberry, in: S.M. Auerbach, K.A. Carrado, P.K. Dutta (Eds.), Handbook of Layered Materials. Marcel Dekker, Inc., New York, 2004, Ch. 8, p. 373.
[12] A. Vaccari. Catal. Today 41(1998), 53.
[13] C.P. Kelkar, A.A. Schutz. Micropor. Mater. 10(1997), 163.
[14] O. Salvador, D. Eva, L. Marta, F. Laura. Catal. Today 167(2011), 71.
[15] L. Marta, D. Eva, V. Aurelio, O. Salvador, A. Aline, Appl. Catal. B: Environ. 102(2011),590.
[16] F. Bergaya, B.K.G. Theng, G. Lagaly, Handbook of Clay Science, Developments in Clay Science, Vol. 1, chapter 3.1, Elsevier, Amsterdam, 2006, p. 1224.
[17] Y.Lwin, M.A.Yarmo, Z.Yaakob, A.B Mohamad, W.A.W.Daud, Mater. Res. Bull.36(2001), 193.
[18] F. Cavani, F. Trifiro, A. Vaccari, Catal. Today 11(1991),173.
[19] V. Rives, O. Prieto, A. Dubey, S. Kannan, J. Catal. 220(2003), 161
[20] L. He, H. Berntsen, E. Ochoa-Fernández , C.J. Walmsley, E.A. Blekkan, D. Chen, Topic Catal. 52(2009), 206 .
[21] V. Rives, in: V. Rives (Ed.), Layered Double Hydroxides: Present and Future, Nova Science, New York, 2001, Ch. 8, p. 229.
[22] O.W.Perez-Lopez, A.Senger, N.R.Marcilio, M.A.Lansarin, Appl. Catal. A: Gen. 303(2006), 234
[23] J.T. Kloprogge, R.L. Frost, in: V. Rives (Ed.), Layered Double Hydroxides: Present and Future, Nova Science, New York, 2001, Ch.5, p. 139.
[24] S. Ribet, D. Tichit, B. Coq, B. Ducourant, F. Morato, J. Solid State Chem. 142(1999), 382
[25] N. A. Hermes, M. A. Lansarin, O. W. Perez-Lopez, Catal. Lett. 141(2011), 1018
[26] L. Chmielarz, P. Kustrowski, A. Rafalska-Lasocha, R. Dziembaj, Thermochim. Acta 395(2003), 225.

Advanced Materials Engineering and Technology

Synthesis of Nano-Structured Ni-Co-Al Hydrotalcites and Derived Mixed Oxides